J Electr Eng Technol.2018; 13(1): 468-475
http://doi.org/10.5370/JEET.2018.13.1.468

ISSN(Print) 1975-0102
ISSN(Online) 2093-7423

Effective Adaptive Dynamic Quadrature Demodulation in Medical Ultrasound Imaging

Heechul Yoon*, Kang-won Jeon*, Hyuntaek Lee*, Kyeongsoon Kim and Changhan Yoon†**

Abstract – In medical ultrasound imaging, frequency-dependent attenuation downshifts and reduces a center frequency and a frequency bandwidth of received echo signals, respectively. This causes considerable errors in quadrature demodulation (QDM), result in lowering signal-to-noise ratio (SNR) and contrast resolution (CR). To address this problem, adaptive dynamic QDM (ADQDM) that estimates center frequencies along depth was introduced. However, the ADQDM often fails when imaging regions contain hypoechoic regions. In this paper, we introduce a valid region-based ADQDM (VR-ADQDM) method to reject the misestimated center frequencies to further improve SNR and CR. The valid regions are regions where the center frequency decreases monotonically along depth. In addition, as a low-pass filter of QDM, Gaussian wavelet based dynamic filtering was adopted. From the phantom experiments, average SNR improvements of the ADQDM and the VR-ADQDM over the traditional QDM were 1.22 and 5.27 dB, respectively, and the corresponding maximum SNR improvements were 2.56 and 10.58 dB. The contrast resolution of the VR-ADQDM was also improved by 0.68 compared to that of the ADQDM. Similar results were obtained from *in vivo* experiments. These results indicate that the proposed method would offer promises for imaging technically-difficult patients due to its capability in improving SNR and CR.

Keywords: Ultrasound imaging, Dynamic quadrature demodulation, Frequency-dependent attenuation

1. Introduction

In conventional medical ultrasound imaging systems, quadrature demodulation (QDM) is commonly utilized to extract envelope information from received radio-frequency (RF) echo signals [1-3]. During the QDM, complex baseband signal is obtained by multiplying cosine and sine waveforms (i.e., down-mixing), where a center frequency of a sinusoidal waveform is typically assumed to be the same as the frequency used in the transmission, followed by a low-pass filter (LPF) to remove high-frequency components. However, a center frequency of echo signal is downshifted and its bandwidth is reduced due to frequency-dependent attenuation as an ultrasound wave propagates through soft tissue [4, 5]. This mismatch between the assumed center frequency and the downshifted received frequency causes the loss of signal-to-noise ratio (SNR). In addition, ultrasound waves traveling a heterogeneous medium attenuate nonlinearly because different types of tissue have different value of attenuation coefficients. Thus, it would be challenging to compensate these varying attenuations with the conventional QDM (CQDM, which uses the constant center frequency and the fixed LPF coefficients.

† Corresponding Author: Dept. of Biomedical Engineering, Inje University, Korea. (cyoon@inje.ac.kr)
* Digital Media & Communications R&D Center, Samsung Electronics Co. Ltd, Korea.
** Dept. of Pharmaceutical Engineering, Inje University Korea.
Received: November 8, 2016; Accepted: September 26, 2017

An adaptive time gain compensator (TGC) can partially compensate the loss in signal strengths occurred by the attenuation [6]. However, the TGC amplifies both noise and echo signals, thus it would make an image noisier if unwanted noise signals are remained after the CQDM. Adaptive dynamic QDM (ADQDM) methods, in which center frequencies along depth are estimated and used during the QDM have been introduced [7, 8]. In the method, a second-order auto-regressive model was employed to estimate a downshift in the center frequency. Then, based on the estimated center frequencies along the depth, ADQDM adaptively selects the frequency for down-mixing at every imaging depth points (or segments) and the LPF coefficients. Similarly, auto-correlation based methods have been also used to track the center frequency downshift [9, 10]. In the methods, the center frequencies were estimated using an analytic signal generated by either the CQDM or the Hilbert transform [11]. After estimating the center frequencies, first- or second-order polynomial fitting were applied to obtain a smooth curve of the estimated center frequency to eliminate fluctuations stemming from coherence noise from sub-resolvable scatterers. The errors of these methods in estimate center frequencies were less than 7% in a homogeneous medium. However, it would be challenging to track down a downshift of center frequency in a heterogeneous medium by using the simple curve fitting method. Furthermore, the center frequencies may under- or over-estimated at low SNR regions, e.g., far depth and hypoechoic regions (e.g.,

Copyright ⓒ The Korean Institute of Electrical Engineers
This is an Open-Access article distributed under the terms of the Creative Commons Attribution Non-Commercial License (http://creativecommons.org/licenses/by-nc/3.0/) which permits unrestricted non-commercial use, distribution, and reproduction in any medium, provided the original work is properly cited.

amniotic fluid or blood).

To obtain a reliable curve of the center frequency, we define a valid region when estimating center frequencies to reject unreliable estimates. For this, it can be assumed that the center frequencies decrease monotonically since the ultrasound wave experiences the frequency-dependent attenuation as it propagates through media [12, 13]. Thus, we estimate center frequencies only in the valid regions. In this paper, we propose an adaptive dynamic QDM method based on a valid region (VR-ADQDM) that can reject the misestimated center frequencies. In addition, an effective fitting method and a dynamic filtering method based on Gaussian wavelet are presented. The proposed method was evaluated through phantoms and in vivo experiments using RF data acquired by a commercial ultrasound machine.

2. Method

In this section, we describe the proposed method, and its effectiveness in estimating center frequencies is examined by computer simulation using Matlab (MathWorks Inc., Natick, MA). In the simulation, beamformed RF data acquired using a commercial ultrasound machine (UGEO H60, Samsung Electronics Co. Ltd., Suwon, Korea) were used. A commercial fetal phantom (SPACEFAN-ST, KYOTO KAGAKU Co. Ltd., Kyoto, Japan) was scanned using a 3-MHz convex array transducer.

2.1 Valid Region-based Adaptive Dynamic Quadrature Demodulation (VR-ADQDM)

Fig. 1(a) shows a block diagram of the proposed VR-ADQDM. Beamformed RF signals, $r(n)$, are first demodulated using CQDM, where a fixed center frequency (typically, transmitted frequency) and filter coefficients are used to obtain complex baseband signal, i.e., $i(n)$ and $q(n)$. Note that the complex baseband signal is not centered at around zero frequency due to a downshift of center frequency. Instantaneous frequencies of the signal are calculated from the complex baseband signal by [10, 11]

$$\Delta f_c(n) = \frac{1}{2\pi T}\tan^{-1}\frac{\sum_{k=-N/2}^{N/2}\left(q(n+k)i(n+k-1)-i(n+k)q(n+k-1)\right)}{\sum_{k=-N/2}^{N/2}\left(i(n+k)i(n+k-1)-q(n+k)q(n+k-1)\right)}, \quad (1)$$

where T is the sampling period and N is the data length of auto-correlation, respectively. From Eq. 1, actual center frequencies of the received echo signal along the imaging depth, $f(n)$, can be obtained by $f_0+\Delta f_c(n)$, where f_0 is the constant frequency used in the CQDM. In the previous

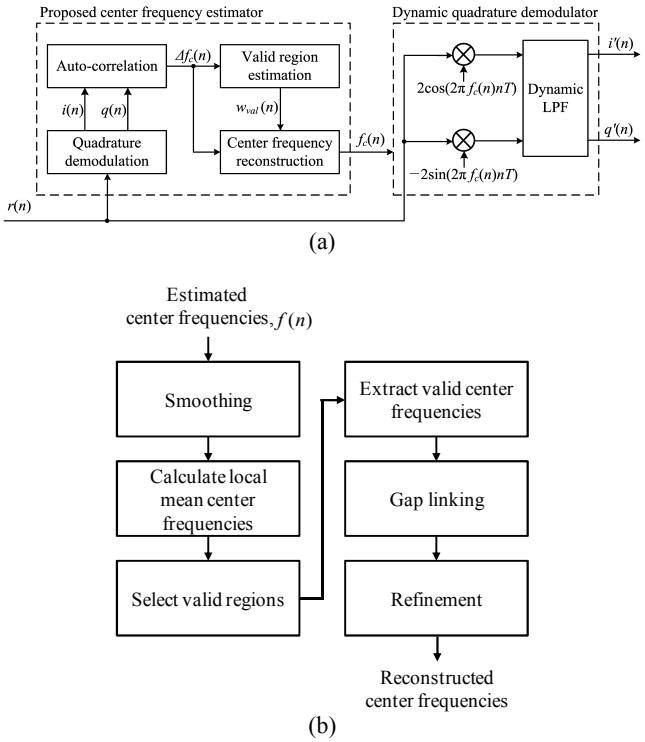

Fig. 1. (a) Overall block diagram of proposed adaptive dynamic quadrature demodulation (VR-ADQDM) and (b) flow chart of center frequency estimation method in the proposed method

methods, a polynomial fitting is performed to obtain a smooth curve along depth using the estimated center frequencies, i.e., $f(n)$ [8-10], which cannot present dynamic attenuation in center frequency in heterogeneous media. In addition, the misestimated center frequencies from regions with low SNR can lead to biased results.

To mitigate these problems, we obtain a final curve of the center frequencies estimated only from the valid regions. A block diagram of the valid region estimate is shown in Fig. 1(b). As can be seen, we applied a three-tap moving average filter which can reject outliers with low computational cost. Then, mean values of local center frequencies are computed, as shown in Fig. 2(a). The validity of estimated center frequencies is determined by a criterion that the center frequencies decrease along imaging depth. In other words, because of fundamental phenomenon of frequency dependent attenuation, the center frequency of an ultrasound wave always downshifts when traveling any media. Thus, based on this physical phenomena, our approach determines increasing estimated frequency as a function of depth as invalid. If the local estimated center frequency is higher than previous one, that position is regarded as the invalid region and thus, their estimates are not used when computing a final curve of center frequency. In this way, we define a valid region map that is a binary map (0 and 1) presenting the validity of each pixel for the frequency estimation. In other words, 0

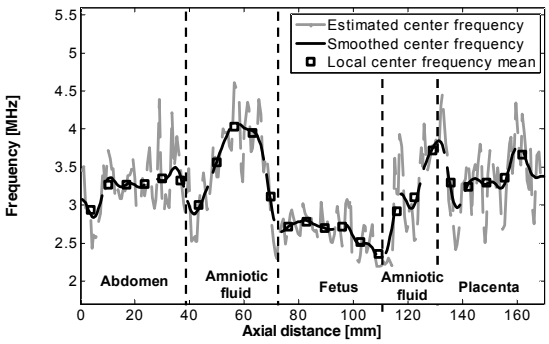

(a)

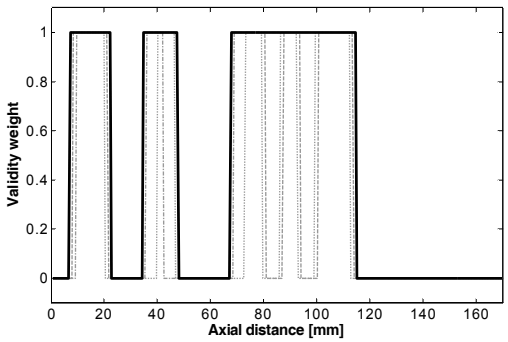

(b)

Fig. 2. Estimation results of (a) center frequencies and (b) valid regions, respectively. These representative results are obtained from a scanline indicated with a white line in Fig. 4(a)

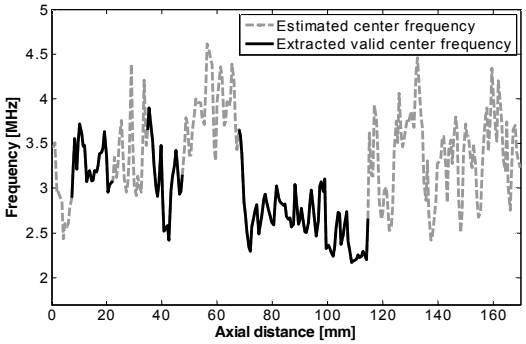

(a)

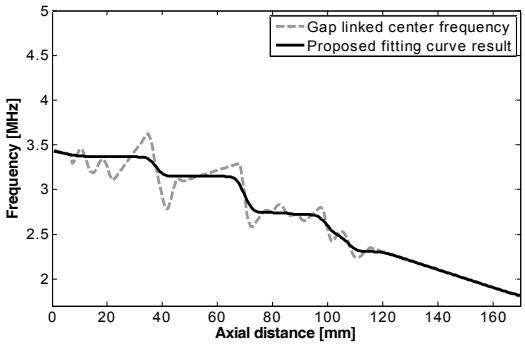

(b)

Fig. 3. Results of center frequency estimation: (a) Estimated center frequencies along with extracted values based on the valid regions and (b) final curve of reconstructed center frequencies along imaging depth

in the map means we cannot use the frequency estimate in that region and vice versa. For the robustness of the method, not only we obtain a single valid region map through this process, but also we repeat this process and obtain multiple valid region maps defined as $w_{val,0}$, $w_{val,1}$, and $w_{val,2}$ Here, we vary the starting points in the computation of valid regions. Then, the final valid region is determined by an inclusive manner, i.e., w_{val}= $w_{val,0} \parallel w_{val,1} \parallel w_{val,2}$, where $\parallel$ denotes the logical OR operation. In our study, three initial points, i.e., depths of 0 , 2, and 4 mm were used. Fig. 2(b) shows the final estimated valid region (black line).

After estimating the valid regions (w_{val}=1), only center frequencies in these valid regions are extracted. The selected center frequencies (black line) are shown in Fig. 3(a). The frequencies in invalid regions (i.e., w_{val}=0) are discarded and they are replaced with the values estimated by linear interpolation and extrapolation of the frequencies extracted in the valid regions. Additional moving averaging is performed to eliminate local peaks, and then a monotonically decreasing curve of center frequency, $f_c(n)$, can be obtained, as shown in Fig. 3(b).

In the proposed VR-ADQDM, the estimated center frequencies, $f_c(n)$, are used not only for down-mixing but also for LPF. The LPF is designed based on a Gaussian wavelet method that was introduced in [14]

$$g(n) = \frac{1}{\sqrt{f_0 / f_c(n)}} \left(\frac{B^2}{2\pi}\right)^{1/4} \exp\left(-\frac{B^2}{4}\left(\frac{n \cdot f_c(n)}{f_0}\right)^2\right), \quad (2)$$

where B is the -6-dB bandwidth of a transducer. After the VR-ADQDM, further signal processing such as envelope detection, log-compression and scan conversion are conducted to obtain B-mode ultrasound images.

2.2 Experiment setup and evaluation metrics

To evaluate the performance of the proposed VR-ADQDM, beamformed RF data from phantoms and in vivo abdominal region were acquired using a commercial ultrasound machine (UGEO H60, Samsung Electronics Co. Ltd., Suwon, Korea) with 3-MHz convex and 5-MHz linear array transducers. In the phantom study, commercial fetal (SPACEFAN-ST, KYOTO KAGAKU Co. Ltd., Kyoto, Japan) and multi-purpose (Model 539, ATS Lab., Bothell, WA, USA) phantoms were scanned. Fractional bandwidths of linear and convex array transducers were, respectively, 60% and 80%, which were used as initial cutoff frequencies for designing dynamic LPFs, i.e., B in Eq. 2. In all experiments, the number of samples for the auto-correlation function (N in Eq. 1) was 64 and a three-tap

moving average filter was utilized for smoothing. To compare the performance, images with the CQDM and ADQDM with a first-order polynomial fitting were also obtained.

For quantitative evaluation, SNR values were measured from phantom and in vivo abdominal data as follows [15]:

$$SNR(d) = 20\log\frac{\max\left[E_{signal}(d)\right]}{std\left[E_{noise}(d)\right]} \tag{3}$$

where d is the depth index, and $E_{signal}(d)$ and $E_{noise}(d)$ are the envelope signals from echo and noise, respectively. The system noise was measured by acquiring beamformed RF data without transmission. In the measurement of SNR, the maximum (i.e., max[·]) and standard deviation (i.e., std[·]) values were obtained within 5 mm of d. In addition, contrast resultion (CR) was computed by using [16]

$$CR = \frac{\left|\mu_l - \mu s\right|}{\left|\sigma_l^2 - \sigma_s^2\right|} \tag{4}$$

where μ_l and μ_s are the mean envelope values from lesion and background speckle regions, respectively, and σ_l and σ_s are their corresponding standard deviation values. The two regions were selected to be the same size and located at the same depth.

3. Results and Discussion

Fig. 4 shows fetal phantom images obtained by the CQDM, the ADQDM, and the VR-ADQDM with a valid region map, respectively. As can be seen in Fig. 4, anatomical features such as fetal body, amniotic fluid, and placenta regions are more clearly visualized when the VR-ADQDM is applied. Especially, the speckle patterns of the placenta region are more pronounced in the proposed method than those in other methods. Noisy signals in the amniotic fluid are also suppressed. The valid region map (Fig. 4(d)) in the proposed VR-ADQDM method shows that it has an ability to reject hypoechogenic regions such as amniotic fluid, fetal heart and stomach. In addition, the placenta region, which locates at the far depth and thus yields low SNR, is successfully excluded.

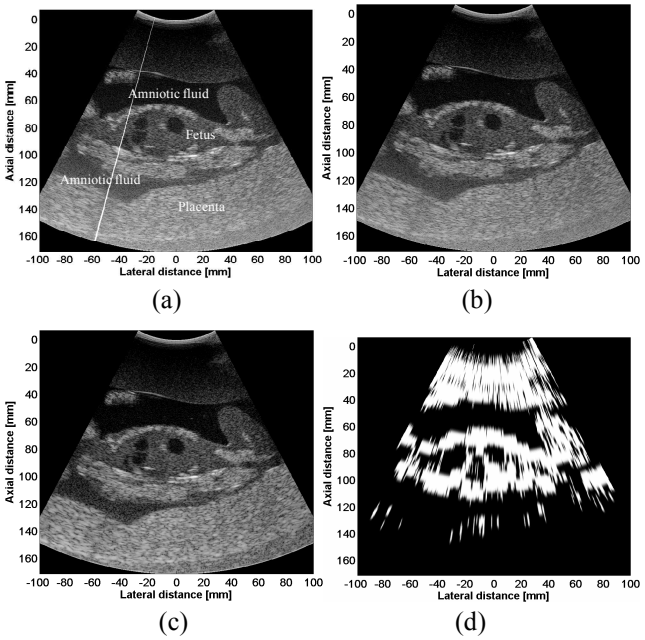

Fig. 4. Fetal phantom images by (a) CQDM, (b) ADQDM, (c) proposed VR-ADQDM methods and (d) its valid region map

Estimated center frequencies along with fitted curves by the conventional ADQDM and VR-ADQDM from a selected scanline (indicated with a white line in Fig. 4(a)) are shown in Fig. 5. As shown in Fig. 5, the center frequencies as a function of depth (gray solid line) were misestimated in the amniotic fluid (depth of 40~70 mm and 110 ~ 130 mm) and placenta (beyond 130 mm) regions. These misestimated values leaded to the erroneous curve fit result in the conventional ADQDM (black dotted line). The slope of fitted curve produced by the ADQDM was almost even along depth. On the other hand, the proposed method could remove those regions, thus the monotonically-decreasing curve (black solid line) could be

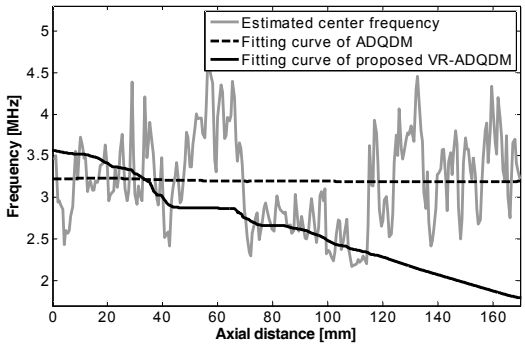

Fig. 5. Estimated center frequencies as a function of depth and reconstructed curve by conventional ADQDM and proposed VR-ADQDM

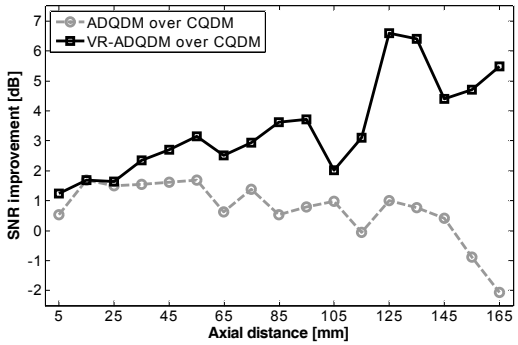

Fig. 6. SNR improvement produced by the conventional ADQDM and proposed VR-ADQDM over CQDM

obtained as shown in Fig. 5. For quantitative comparison, SNR improvements of the ADQDM and the VR-ADQDM over the CQDM were measured and plotted in Fig. 6. Here, the maximum SNR improvements of the ADQDM and VR-ADQDM were 1.69 and 6.58 dB, respectively, and the mean improvements were 0.71 and 3.42 dB for each method.

Phantom images processed by the CQDM, the ADQDM, and the VR-ADQDM along with a valid region map are, respectively, shown in Fig. 7. Holes at far depths could be visualized in the image produced by the proposed method whereas they are not visible in the images created by the CQDM and the ADQDM. This can be explained from results of the center frequency estimate, which is shown in Fig. 8. The estimated center frequencies (gray line) first decreased, and increased after depth of 110 mm due to low SNR at far depth, resulting in an increasing fitting curve in the ADQDM. On the other hand, a curve produced by the proposed method could track down the estimated center frequencies since it only utilize the center frequencies from valid regions (Fig. 7(d)) when generating the curve.

Improvements of SNR and CR over the CQDM are presented in Fig. 9. The CR values were measured from holes and adjacent speckle regions, which are indicated with white boxes in Fig. 7(a). As can be seen, the improvement of SNR and CR in the proposed method was higher than those by the ADQDM. The average SNR improvements of ADQDM and VR-ADQDM were,

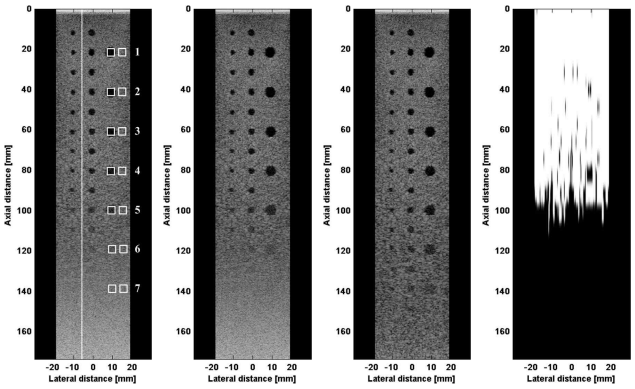

(a) (b) (c) (d)

Fig. 7. Phantom images by (a) CQDM, (b) ADQDM, (c) proposed VR-ADQDM and (d) its valid region map

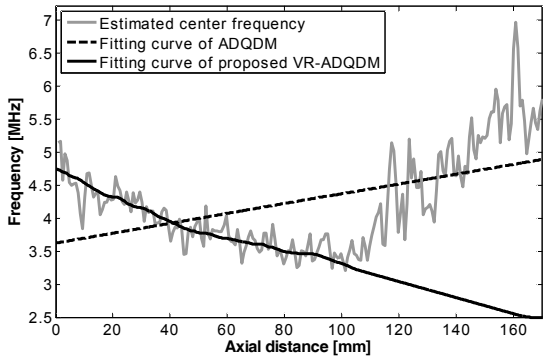

Fig. 8. Estimated center frequencies and reconstructed curves by the conventional ADQDM and proposed method

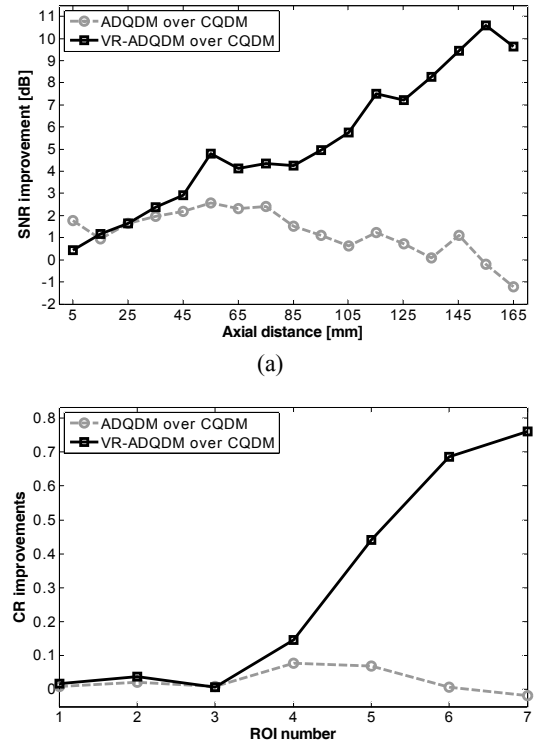

(a)

(b)

Fig. 9. Improvement of (a) SNR and (b) CR produced by the conventional ADQDM and proposed VR-ADQDM over CQDM

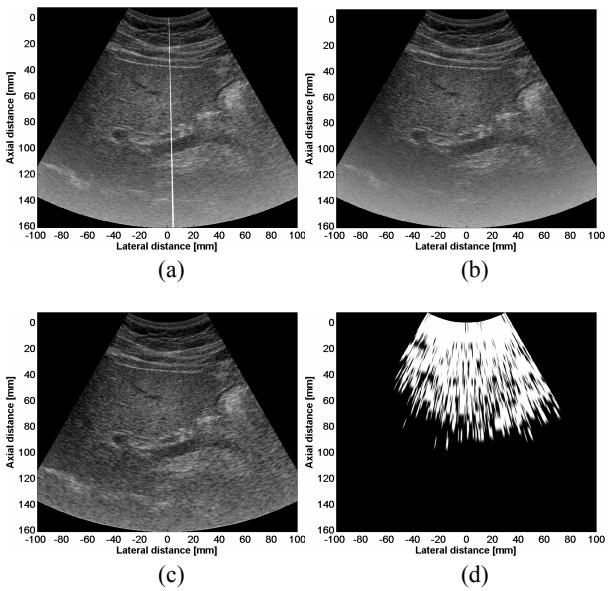

(a) (b)

(c) (d)

Fig. 10. In vivo liver images by (a) CQDM, (b) ADQDM, (c) proposed VR-ADQDM and (d) its valid region map

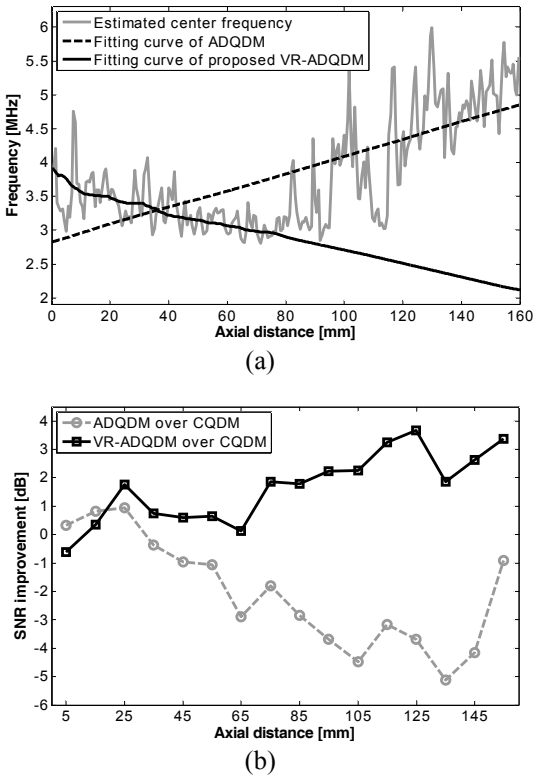

Fig. 11. (a) Estimated center frequencies and reconstructed curve by conventional ADQDM and proposed VR-ADQDM and (b) SNR improvement of each method over the conventional QDM

respectively, 1.22 and 5.27 dB, and the maximum improvements for each method were 2.56 and 10.58 dB. The average CR improvements for the ADQDM and VR-ADQDM were 0.02 and 0.30, respectively, and the maximum values were 0.08 and 0.76.

Fig. 10 and 11 show in vivo liver images produced by each method, and resultant curves of estimated center frequency and SNR improvement, respectively. As shown in Fig. 11(a), the curves by the ADQDM and VR-ADQDM were similar to the results from the phantom experiments; the curve of center frequency in the ADQDM increased due to low SNR at the far region whereas the curve by the proposed method decreased. This misestimated curve leaded to inadequate down-mixing and broadening the bandwidth of the LPF, reducing the SNR in the ADQDM, as shown in Fig. 11(b). The average and maximum SNR improvement of the proposed method were 1.66 and 3.66 dB, respectively.

From the phantom and in vivo experiments, we demonstrated that the proposed VR-ADQDM method could improve the SNR and the CR over the conventional methods. Thus, our method is expected to be useful for imaging technically-difficult patients. Although the proposed method requires additional computation for estimating center frequencies along imaging depth, its burden would not be considerable since it only utilized simple computations, g, auto-correlation, moving average, linear interpolation and extrapolation. This computational complexity can be handled with modern multi-core processors such as a central processing unit or a graphic processing unit.

4. Conclusion

In the paper, we have proposed the VR-ADQDM method that can effectively remove the misestimated center frequencies and thus create a reliable curve for the downshiting frequencies along the depth. In the method, the center frequency curve was obtained from the frequency estimates computed only in the valid regions under an assumption that the center frequencies decrease as ultrasound waves propagate through biological tissue. The performance of the proposed method was assessed through the phantom and in vivo experiments. We demonstrated that the proposed VR-ADQDM method outperformed in improving signal-to-noise ratio and contrast resolution compared to the conventional methods, i.e., conventional QDM and ADQDM.

Acknowledgements

This work has been supported by the 2016 Inje University research grant.

References

[1] J. H. Chang, J. T. Yen and K. K. Shung, "A novel envelope detection for high-frame rate, high-frequency ultrasound imaging," *IEEE Trans. Ultrason. Ferroelect. Freq. Control.*, vol. 54, no, 9, pp. 1792-1801, 2007.

[2] G.-D. Kim, C. Yoon, S. -B. Kye, Y. Lee, J. Kang, Y. Yoo and T. -K. Song, "A single FPGA-based portable ultrasound imaging system for point-of-care applications," *IEEE Trans. Ultrason. Ferroelect. Freq. Control.*, vol. 59, no. 7, pp. 1386-1394, 2012.

[3] J. Kang, C. Yoon, J. Lee, S. Kye, Y. Lee, J. H. Chang, G. Kim, Y. Yoo and T.-K. Song, "A system-on-chip solution for point-of-care ultrasound imaging systems: Architecture and ASIC implementation," *IEEE Trans. Biomed. Circuits Syst.*, vol. 10, no. 2, pp. 412-423, 2016.

[4] T. Baldweck, P. Laugier, A. Herment and G. Berger, "Application of autoregressive spectral analysis for ultrasound attenuation estimation: interest in highly attenuating medium," *IEEE Trans. Ultrason. Ferroelectr. Freq. Control.*, vol. 42, no. 1, pp. 99-110, 1995.

[5] J. A. Jensen, Estimation of Blood Velocities using Ultrasound: A Signal Processing Approach, Cambridge University Press, Cambridge, UK, 1996, pp. 29-191.

[6] S. D. Pye, S. R. Wild and W. N. McDicken, "Adaptive time gain compensation for ultrasonic imaging," *Ultrasound Med. Biol*., vol. 18, no. 2, pp. 205-212, 1992.
[7] J. Girault, F. Ossant, A. Ouahabi, D. Kouname and F. Patat, "Time-varying autoregressive spectral estimation for ultrasound attenuation in tissue characterization," *IEEE Trans. Ultrason. Ferroelectr. Freq. Contr*., vol. 45, no. 3, pp. 650-659, 1998.
[8] D.Y. Lee, Y. Yoo, T.K. Song and J.H. Chang, "Adaptive dynamic quadrature demodulation with autoregressive spectral estimation in ultrasound imaging," *Biomed. Signal Proces*., vol. 7, no. 4, pp. 371-378, 2012.
[9] N. Feng, J. Zhang and W. Wang, "A quadrature demodulation method based on tracking the ultrasound echo frequency," *Ultrasonics*, vol. 44, pp. e47-e50, 2006.
[10] C. Yoon, G. -D. Kim, Y. Yoo, T. -K. Song and J. H. Chang, "Frequency equalized compounding for effective speckle reduction in medical ultrasound imaging," *Biomed. Signal Proces*., vol. 8, no. 6, pp. 876-887, 2013.
[11] G. Park, S. Yeo, J. J. Lee, C. Yoon, H. -W, Koh, H. Lim, Y. Kim, H. Shim and Y. Yoo, "New adaptive clutter rejection based on spectral analysis for ultrasound color Doppler imaging: Phantom and in vivo abdominal study," *IEEE Trans. Biomed. Eng*., vol. 61, no. 1, pp. 55-63, 2014.
[12] M. Fink, F. Hottier and J. F. Cardoso, "Ultrasonic signal processing for in vivo attenuation measurement: Short time Fourier analysis," *Ultrason. Imaging*, vol. 5, no. 2, pp. 117-135, 1983.
[13] M.O. Culjat, D. Goldenberg, P. Tewari and R.S. Singh, "A review of tissue substitutes for ultrasound imaging," *Ultrasound Med. Biol*., vol. 36, no. 6, pp. 861-873, 2010.
[14] P. Wang, Y. Shen and Q. Wang, "Gaussian wavelet based dynamic filtering (GWDF) method for medical ultrasound systems," *Ultrasonics*, vol. 46, no. 2, pp. 168-176, 2007.
[15] K.F. Üstüner and G.L. Holley, Ultrasound imaging system performance assessment, AAPM 45th Annual Meeting, San Diego, CA, 2003, pp. 10-14.
[16] C. Yoon, Y. Lee, J. H. Chang, T. -K. Song and Y. Yoo, "In vitro estimation of mean sound speed based on minimum average phase variance in medical ultrasound imaging," *Ultrasonics*, vol. 51, no. 7, pp. 795-802, 2011.

Heechul Yoon received his B.S. and M.S. degrees in electrical engineering from the Sogang University, Seoul, South Korea in 2008 and 2010, respectively. From 2010 to 2014, he worked in Samsung Electronics, Suwon, South Korea as a researcher on ultrasound signal and image processing. In 2014, he began his Ph.D. studies at the University of Texas at Austin where he conducted studies in the Ultrasound Imaging and Therapeutics Laboratory. In 2015, the laboratory moved to the Georgia Institute of Technology where he is pursuing Ph.D. studies in Electrical and Computer Engineering. He conducts his research at Georgia Tech and Emory University School of Medicine. His research interests include development and clinical translation of medical imaging technologies including shear wave elasticity imaging and ultrasound-guided photoacoustic imaging.

KangWon Jeon received his B.S. and M.S. degrees in electrical engineering from the Sogang University, Seoul, South Korea in 2010 and 2012, respectively. From 2012 to 2013, he worked in Continental Automotive Systems Korea, Icheon, South Korea as a development engineer for automotive safety solution. In 2013, he moved to Samsung Electronics, Suwon, South Korea as a researcher on ultrasound signal and image processing. His research interests include development and clinical measurement accuracy of medical imaging technologies including ultrasound high-resolution imaging and Doppler imaging system.

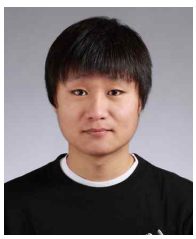

Hyuntaek Lee received his B.S. and M.S. degrees in electrical engineering from the Sogang University, Seoul, South Korea in 2008 and 2010, respectively. In 2010, he begun working in Samsung Electronics, Suwon, South Korea as a researcher on ultrasound signal and image processing. His research interest include development and improve quality of medical imaging technologies including ultrasound imaging system and image processing.

Kyeongsoon Kim received B.S. degree in Pharmacy from the Ehwa Womans University, Seoul, Korea, and M.S and Ph.D degrees in Pharmaceutical Analytical Chemistry from Seoul National University, Seoul, Korea. She is currently an Assistant Professor in the Department of Pharmaceutical Engineering at Inje University. Her research interests include Clinical study developing and management, Regulatory affairs for new drug development, Clinical pharmacology, and Drug environmental monitoring.

Changhan Yoon received his M.S. and Ph.D. degrees in electronic engineering from Sogang University, Seoul, South Korea, in 2009 and 2013, respectively. He was a Postdoctoral Research Associate with the NIH Resource Center for Medical Ultrasonic Transducer Technology, University of Southern California, Los Angeles, CA, USA, and was a Postdoctoral Fellow with the Georgia Institute of Technology, Atlanta, GA, USA. He is currently an Assistant Professor in the Biomedical Engineering at Inje University, Gyengnam, Korea. His current research interests include medical ultrasound and photoacoustic imaging systems and their clinical applications and ultrasound microbeams.